Applied Surface Science Advances 5 (2021) 100098

Contents lists available at ScienceDirect

Applied Surface Science Advances

journal homepage: www.elsevier.com/locate/apsadv

Enzyme-mediated film formation of melanin-like species from *ortho*-diphenols: Application to single-cell nanoencapsulation

Nayoung Kim[a,†], Hojae Lee[a,†], Sang Yeong Han[a], Beom Jin Kim[b,*], Insung S. Choi[a,*]

[a] Department of Chemistry, KAIST, Daejeon 34141, South Korea
[b] Department of Chemistry, University of Ulsan, Ulsan 44610, South Korea

ARTICLE INFO

Keywords:
Single-cell nanoencapsulation
Melanogenesis
Glucose oxidase
Horseradish peroxidase
ortho-Diphenols

ABSTRACT

Single-cell nanoencapsulation (SCNE) is a nanoarchitectonic strategy for creating cell-in-shell structures, in which the artificial shells, formed on individual living cells, protect the cells inside from otherwise lethal factors and also potentially provide them with advanced functions, such as exogenous biochemical reactions that are not attainable in wild-type cells. This work investigated enzymatic cascade systems for widening the substrate scope, beyond catecholamines, in the in-vitro formation of melanin-like films and shells and, ultimately, providing advanced building blocks and tools to the field of SCNE, inspired by the enzyme-derived structural diversification of melanin found in nature. The combination of glucose oxidase and horseradish peroxidase enabled the facilitated film formation of amine group-absent *ortho*-diphenols, such as protocatechuic aldehyde (PCA) and pyrocatechol. As a proof-of-demonstration, the developed reaction protocol was applied to the cytocompatible SCNE of *Saccharomyces cerevisiae*.

1. Introduction

Natural materials and their synthetic processes found in biological organisms have ceaselessly been inspiring researchers to chemically mimic the materials and processes for advanced construction of functional materials that are structurally exquisite [1–4]. This paper describes our recent research efforts that mimic the melanin formation ("melanogenesis") for constructing nanoarchitectonic cell-in-shell structures in single-cell nanoencapsulation (SCNE), in which nature-mimetic artificial shells formed on individual cells endow the cells with exogenous properties including cytoprotective capability [5–7].

Cytoprotection is a notable function of melanin. For example, insects utilize melanin as a skeletal component, which hardens the cuticles and, of more importance, quarantines pathogens and damaged tissues [8,9]. Certain microbes make themselves highly resistant to lethal stressors, such as reactive oxygen species (ROS) and microbicides, by constructing melanin-based coats on cell surfaces [10,11]. In human, melanin, as a primary determinant of skin and hair color, ameliorates the damage by UV radiation [12]. Early examples of melanogenesis-inspired SCNE include the cytoprotective encapsulation of individual *Saccharomyces cerevisiae* within polydopamine shells [13].

Melanin is broadly defined as a set of highly irregular heteropolymers mainly composed of the monomeric units derived from the enzymatic oxidation of an amino acid, L-tyrosine (L-Tyr). It is thought that the functions of melanin are augmented by its diversified substructures, exemplified by eumelanin and pheomelanin [14,15]. Melanogenesis typically starts with hydroxylation of L-Tyr to L-DOPA (L-3,4-dihydroxyphenylalanine), followed by its oxidation to DOPAquinone (Fig. 1) [16]. In the case of eumelanin formation, DOPAquinone undergoes intramolecular cyclization to leukodopachrome, which is then oxidized to DOPAchrome. The next melanogenetic pathway consists of several spontaneous reactions under oxidizing conditions: conversion DOPAchrome to 5,6-dihydroxyindole (DHI) or 5,6-dihydroxyindole-2-carboxylic acid (DHICA), oxidation of DHI or DHICA to its corresponding indolequinone, and polymerization to eumelanin. All the reaction steps are tightly controlled by a series of tyrosinase family, and tyrosinase is a key enzyme that catalyzes both hydroxylation of L-Tyr and subsequent oxidation to DOPAquinone, as well as oxidation of DHI to the indolequinone [17–19].

Tyrosinase directly transfers two electrons produced during oxidative catalytic reactions to molecular oxygen, leading to water formation [20]. As a result, the production of ROS and semi-quinone radicals is enormously reduced, which minimizes cellular damage during melanogenesis. Inspired by the intimate involvement of tyrosinase in melanogenesis [21], we have previously proposed the in-vitro use of tyrosinase in the film formation of melanin-like species (MLS) at neutral pH in the aqueous solution and applied the tyrosinase-catalyzed film formation to the melanogenesis-inspired SCNE [22]. Al-

* Corresponding authors.
E-mail addresses: kimbj@ulsan.ac.kr (B.J. Kim), ischoi@kaist.ac.kr (I.S. Choi).
† These authors contributed equally to this work.

https://doi.org/10.1016/j.apsadv.2021.100098
Received 9 February 2021; Received in revised form 23 March 2021; Accepted 4 April 2021

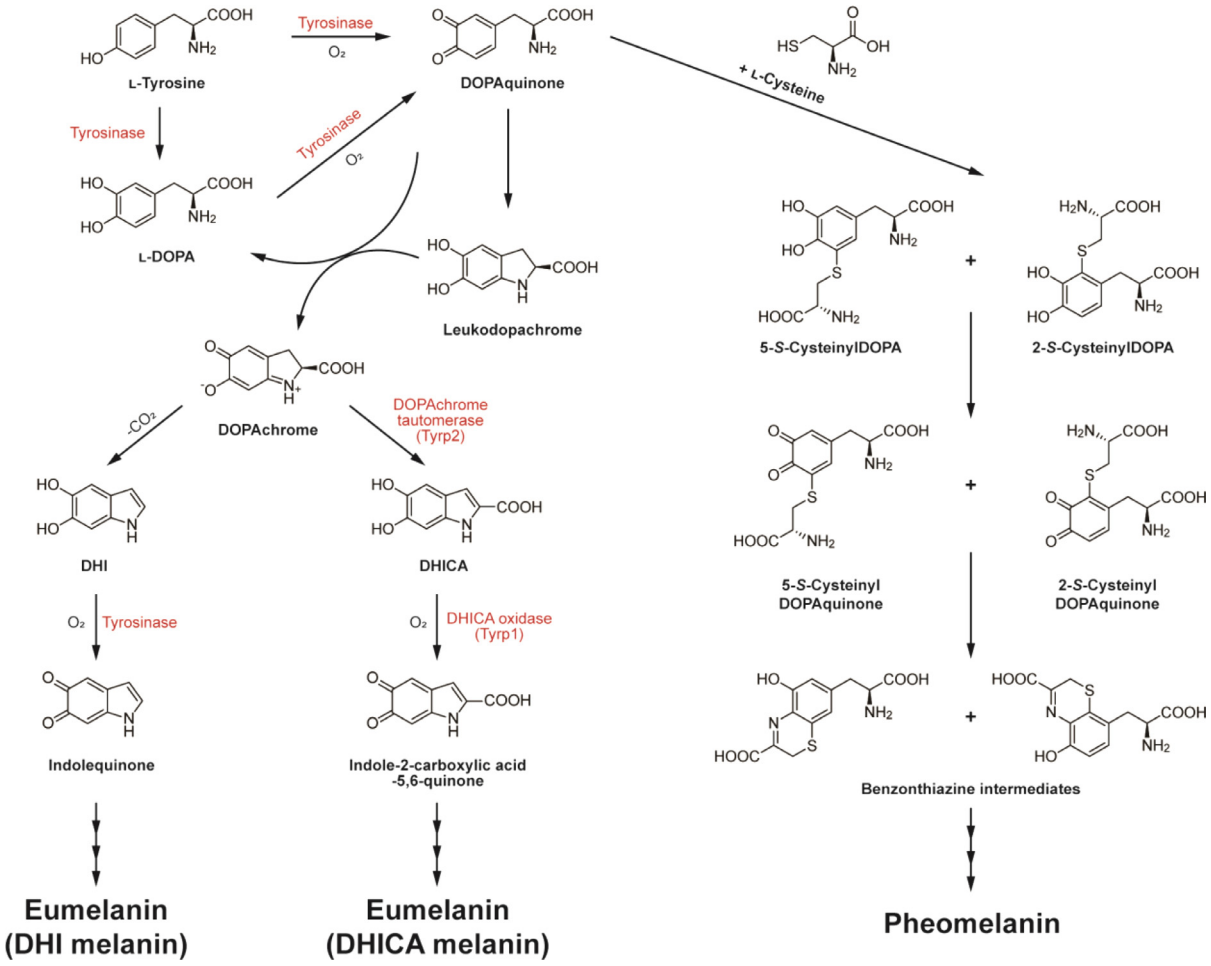

Fig. 1. Examples of melanogenesis pathways. Tryp: tyrosinase-related protein.

though it was found in the study that tyrosinase accepted phenolic amines, such as L-Tyr, L-DOPA, dopamine (4-(2-aminoethyl)benzene-1,2-diol), L-norepinephrine (4-[(1*R*)-2-amino-1-hydroxyethyl]benzene-1,2-diol) and tyramine (4-(2-aminoethyl)phenol), as a coating precursor, the substrate scope for film formation was still limited, critically requiring the presence of amine groups in the substrate structures. For example, no films were formed with protocatechuic aldehyde (3,4-dihydroxybenzaldehyde), pyrocatechol (benzene-1,2-diol), pyrogallol (benzene-1,2,3-triol), and gallic acid (3,4,5-trihydroxybenzoic acid). It is envisaged that the methodological development for expanding the substrate scope in melanogenesis-inspired formation of films and shells to general *ortho*-diphenols (*o*-diphenols) would advance the nanoarchitectonic construction of cellular hybrid systems [23,24].

The formation of pheomelanin—another type of melanin—includes the coupling reaction of DOPAquinone with thiol-containing compounds, such as L-cysteine and glutathione, instead of its intramolecular cyclization to leukodopachrome [25]. Melanin structure is further diversified by incorporation of different monomer units, including 1,8-dihydroxynaphthalene (DHN), 4-hydroxyphenyl pyruvate and dopamine [26–28], and additional involvement of other compounds as additives, such as *N*-acetyldopamine and *N*-β-alanyldopamine [29]. Correspondingly, various enzymes, including laccase and phenoloxidase, are involved in the structural diversification of melanin [30]. The enzyme-mediated diversification strategy inspired us to investigate the use of enzymes other than tyrosinase for widening the substrate scope in the MLS production in SCNE. In this work, we showed that the combination of glucose oxidase (GOx) and horseradish peroxidase (HRP) facilitated the MLS formation of *o*-diphenols (e.g., protocatechuic aldehyde and pyrocatechol), and applied the established reaction protocol to the cytocompatible SCNE of *S. cerevisiae*.

2. Experimental procedure

2.1. Materials

L-Tyrosine (L-Tyr, ≥ 98%), L-3,4-dihydroxyphenylalanine (L-DOPA, 98%), L-norepinephrine hydrochloride (L-NE, ≥ 97%), pyrocatechol (PC, ≥ 99%), protocatechuic aldehyde (PCA, 97%), gallic acid (GA, ≥ 98%), glucose oxidase (GOx, from *Aspergillus niger*), horseradish peroxidase (HRP, from *Amoracia rusticana*), D-(+)-glucose (Glu, ≥ 99.5%), fluorescein diacetate (FDA), fluorescein isothiocyanate-conjugated dextran (FITC-conjugated dextran, MW: 4, 20, or 250 kDa), and tetrahydrofuran (THF) were purchased from Sigma-Aldrich and used as received. Yeast-extract-peptone-dextrose broth (YPD broth, Duchefa Biochemistry), yeast-extract-peptone-dextrose agar (YPD agar, Duchefa Biochemistry), phosphate-buffered saline (PBS, pH 7.4, Welgene), penicillin-streptomycin (P/S, 5000 U mL^{-1} of penicillin and 5000 mg mL^{-1} of streptomycin, Welgene), ethanol (EtOH, 95.0%, Samchun), acetone (99.5%, Samchun), hydrogen peroxide (H_2O_2, 34.5%, Samchun), and polystyrene (PS) beads (diameter: 3.97 μm, microparticles GmbH) were used as received. Gold (Au) substrates were prepared by thermal deposition of Ti (5 nm) and Au (100 nm) onto silicon wafers (Sehyoung

Wafertech). Deionized (DI) water (18.3 MΩ·cm) from Milli-Q Direct 8 (Millipore) was used.

2.2. Enzyme-mediated formation of MLS films

An *o*-diphenol compound (PCA, PC, L-DOPA, L-NE, GA, or L-Tyr) was dissolved in PBS (concentration: 0.8 mg mL^{-1}). After addition of GOx (1 U mL^{-1}) and HRP (0.2 U mL^{-1}), the resulting solution was mixed with the PBS solution of Glu (20 mM) with 1:1 volume ratio (final concentrations: [*o*-diphenol] = 0.4 mg mL^{-1}, [GOx] = 0.5 U mL^{-1}, [HRP] = 0.1 U mL^{-1}, and [Glu] = 10 mM). After predetermined time of reaction (0, 5, 15, 30, 45, 60, 90, 120, 150, 180, 240, 300 or 360 min), 50 μL of an aliquot was taken from the reaction solution, diluted in 950 μL of PBS, and analyzed with a UV-vis spectrophotometer (UV-2550, Shimadzu). For MLS film formation, Au substrates were immersed in the 3-mL solution of *o*-diphenol (0.4 mg mL^{-1}), GOx (0.5 U mL^{-1}), HRP (0.1 U mL^{-1}), and Glu (10 mM), and the samples were placed on an orbital shaker with 120 rpm at 33 °C. After pre-determined time of reaction (15, 30, 45, 60, 90, 120, 180, 240, 300, and 360 min), the Au substrates were washed with DI water and dried under a stream of Ar gas. The film thickness was calculated with a spectroscopic ellipsometer (Elli-SE, Ellipso Technology Co.). Polarized infrared external reflectance spectroscopy (PIERS) spectra of the films were recorded with a nitrogen-purged Fourier-transform infrared (FT-IR) spectrophotometer (Nexus 670, Thermo Nicolet): PIERS spectra were equalized by adding approximately 2000 scans for background and each sample. X-ray photoelectron spectroscopy (XPS) spectra of the films were acquired with a surface analysis instrument (Sigma Probe, Thermo VG Scientific). The morphology of the MLS films was characterized with a scanning electron microscope (SEM, F50, FEI). For contact angle measurement, 3 μL of an aqueous droplet was positioned on a native Au substrate or the MLS-coated Au substrate, and the water contact angle was measured based on the optical image of the droplet.

2.3. Single-cell nanoencapsulation of S. cerevisiae with $MLS_{[PCA]}$

For preparation of yeast@$MLS_{[PCA]}$, a single colony of *S. cerevisiase* (baker's yeast) was picked from a YPD agar plate, suspended in the YPD broth, and cultured in a shaking incubator at 33 °C for 30 h. Prior to shell formation, the cells were washed with DI water three times. To a pellet of *S. cerevisiase* were added sequentially the PBS solutions of PCA (0.8 mg mL^{-1}; 4 mL), Glu (20 mM; 4 mL), GOx (400 U mL^{-1}; 10 μL) and HRP (80 U mL^{-1}; 10 μL), and the mixture was then incubated at 33 °C for 6 h. Yeast@$MLS_{[PCA]}$ cells were washed with DI water at least three times to remove any residual chemicals. The cell viability was investigated with FDA. FDA was dissolved in acetone at the concentration of 10 mg mL^{-1} for preparation of a FDA stock solution, and 5 μL of the FDA stock solution was mixed with 1 mL of a cell suspension in PBS for 15 min at 33 °C while shaking. The cells were collected by centrifugation, washed with DI water, and characterized with a confocal laser-scanning microscope (CLSM, LSM 700, Carl Zeiss) and the SEM. For thickness measurement and permeability analysis of $MLS_{[PCA]}$ shells, hollow $MLS_{[PCA]}$ capsules were fabricated with polystyrene (PS) beads (diameter: 3.97 μm) as a sacrificial template. PS beads were suspended in the enzyme-mediated reaction solution of PCA (0.8 mg mL^{-1}; 4 mL), Glu (20 mM; 4 mL), GOx (400 U mL^{-1}; 10 μL) and HRP (80 U mL^{-1}; 10 μL), and the mixture was placed in a shaking incubator at 33 °C for 6 h. The resulting PS@$MLS_{[PCA]}$ were washed with DI water at least three times to remove any residual chemicals, and the sacrificial PS was dissolved with THF for formation of hollow $MLS_{[PCA]}$ capsules. The hollow capsules were spread on a glass substrate and dried under air for 12 h, followed by shell-thickness measurement with an atomic force microscope (AFM, JPK model: NanoWizard4, Bruker). For permeability analysis, the hollow $MLS_{[PCA]}$ capsules were incubated in an aqueous solution of FITC-conjugated dextran (1 mg mL^{-1}; MW: 4, 20, or 250 kDa). After 10 min of incubation, the penetration of FITC-conjugated dextrans into the capsules was monitored by CLSM.

3. Results and discussion

3.1. Reaction of protocatechuic aldehyde (PCA) and L-DOPA with GOx and HRP in solution

We used a combination of GOx and HRP for the enzyme-mediated MLS production from *o*-diphenols. In this design of enzyme sets, GOx first catalyzes the oxidation of D-(+)-glucose (Glu) in the presence of atmospheric molecular oxygen (O_2) and generates H_2O_2 as one of its reaction products. HRP then oxidizes *o*-diphenols, with an aid of H_2O_2, and converts them into MLS (Fig. 2a). We anticipated that the control over H_2O_2 level would determine the formation of thin, self-adherent MLS films and shells. Although it was reported that the use of only HRP accelerated the oxidative polymerization of dopamine under the basic pH (pH 8.5) [31], HRP-mediated film formation and its substrate scope have not been reported yet, not to mention the reaction performance at the physiological pH (pH 7.4).

We first investigated the performance characteristics of the designed enzyme system with protocatechuic aldehyde (3,4-dihydroxybenzaldehyde; PCA) as a model precursor for *o*-diphenols that do not bear amine groups (Fig. 2b). PCA is a natural *o*-polyphenol composed of 1,2-dihydroxybenzene (a.k.a., catechol or pyrocatechol) and aldehyde groups, which is found in barley, grapevine leaves, green bananas, *Salvia miltiorrhiza* root, and *Phellinus linteus*. A PBS solution of PCA was prepared at pH 7.4, followed by sequential addition of GOx, HRP, and Glu (Refer to the experimental procedure for the concentrations). The solution gradually turned to brown over time, indicative of $MLS_{[PCA]}$ formation (Fig. 2c). The increment of peak intensity at 420 nm, along with the decrement of the peaks at 250 and 345 nm from PCA, in the time-lapse UV-visible spectra suggested the in-situ formation of PCA-derived quinone intermediates (Fig. 2d) [32]. The peaks at 225 and 275 nm implied that the formed $MLS_{[PCA]}$ might contain poly(catechol) and heterocyclic moieties, such as benzoin or stilbenediol [33]. After 6 h of incubation, the brownish MLS precipitated, and neither water nor organic solvent (i.e., methylene chloride) could dissolve them, like biologically generated melanin (Fig. 2e).

We also studied the reaction characteristics of L-DOPA, which is one of the important intermediates in biological melanogenesis (Fig. S1). Upon addition of GOx, HRP, and Glu, the L-DOPA solution gradually turned to pale orange, and the solution color was intensified to dark brown. The peak appearance at 310 and 480 nm in the UV-visible spectra indicated the generation of the intermediates in the melanogenesis pathway, including DOPAquinone and DOPAchrome. Taken together, the solution-based analyses clearly confirmed that the combination of GOx and HRP was versatile in the MLS formation under physiologically relevant conditions.

3.2. Film formation with PCA and L-DOPA on gold

The enzyme-mediated film formation from PCA was investigated with flat gold (Au) substrates as a model, and followed by spectroscopic ellipsometry (Fig. 3a). The ellipsometric analysis showed the sigmoidal film-growth curve: for example, after short lag-phase (< 1 h), the film thickness sharply increased to 22.0 nm at 4 h of reaction and the thickness increase slowed down afterwards. The film of PCA-derived MLS ($MLS_{[PCA]}$) was further characterized by SEM, contact-angle measurement, PIERS, and XPS. After $MLS_{[PCA]}$ film formation, the Au substrate became rougher, composed of nanoparticulates, which indicated the successful film formation (Fig. 3b). The change in static water contact angle, from 66.8° to 41.1°, also confirmed the film formation (Fig. 3c). The PIERS analysis indicated the presence of $MLS_{[PCA]}$ in the film: the spectrum contained the signature peaks of melanin at 1276, 1419, 1617 and 1685, and 3334 cm^{-1}, corresponding to ether (C–O–C), alkene (C=C), carbonyl (C=O), and hydroxyl (O–H) groups, respectively (Fig. 3d). The C 1s XPS spectrum could be deconvoluted into three peaks

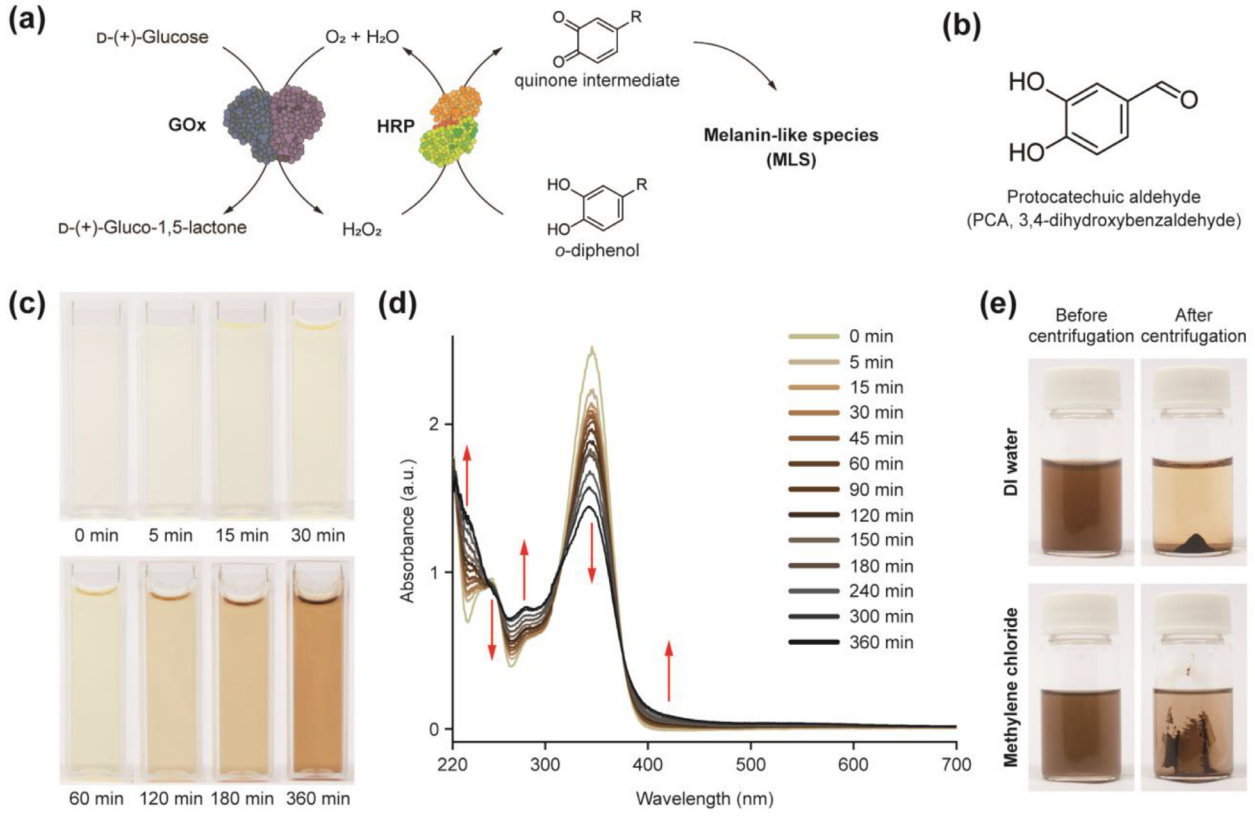

Fig. 2. (a) Schematic for GOx/HRP-mediated cascade reactions for synthesis of MLS from *o*-diphenols. (b) Molecular structure of protocatechuic aldehyde (PCA). (c) Time-lapse optical images and (d) UV-visible spectra of the PCA solution after addition of GOx, HRP, and D-(+)-glucose (Glu). (e) Optical images of the precipitated $MLS_{[PCA]}$ in (top) water and (bottom) methylene chloride: before and after centrifugation.

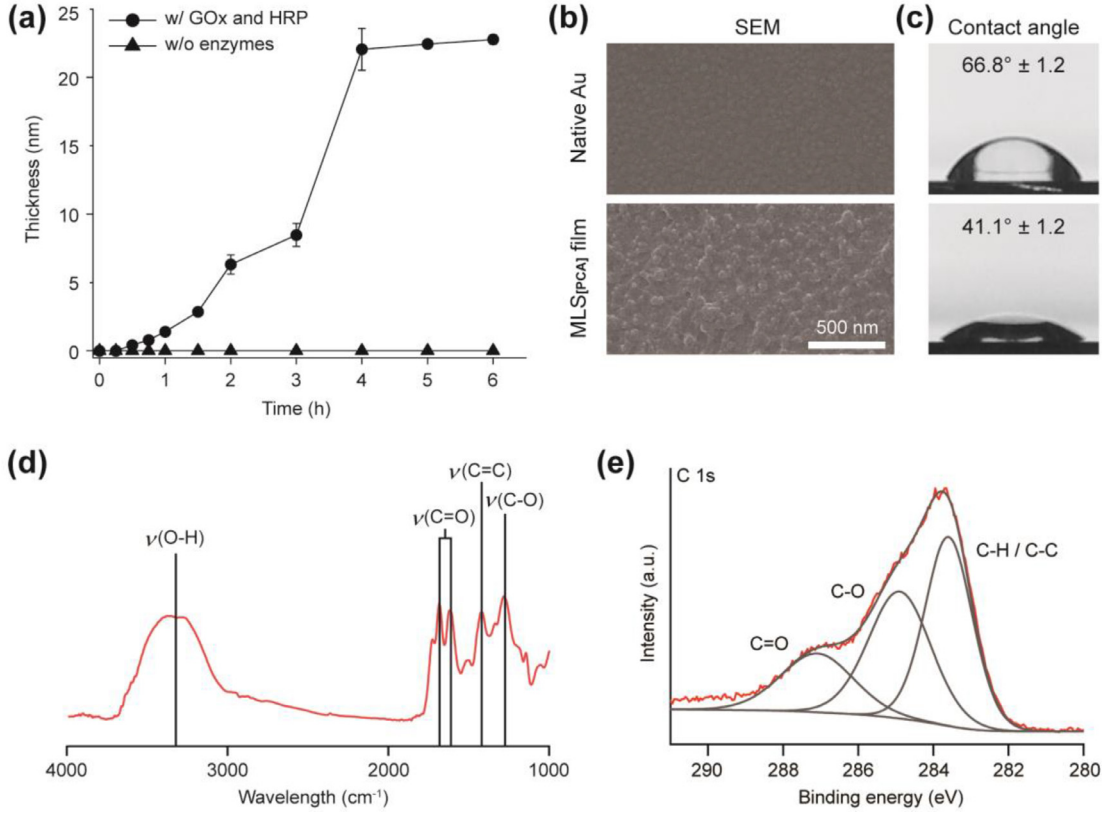

Fig. 3. Characterizations of $MLS_{[PCA]}$ films. (a) Graph of film thickness versus reaction time. (b and c) SEM images of films and (c) optical images of water droplets. Control: native Au substrate. (d and e) PIERS and (e) C 1s XPS spectra of $MLS_{[PCA]}$ films.

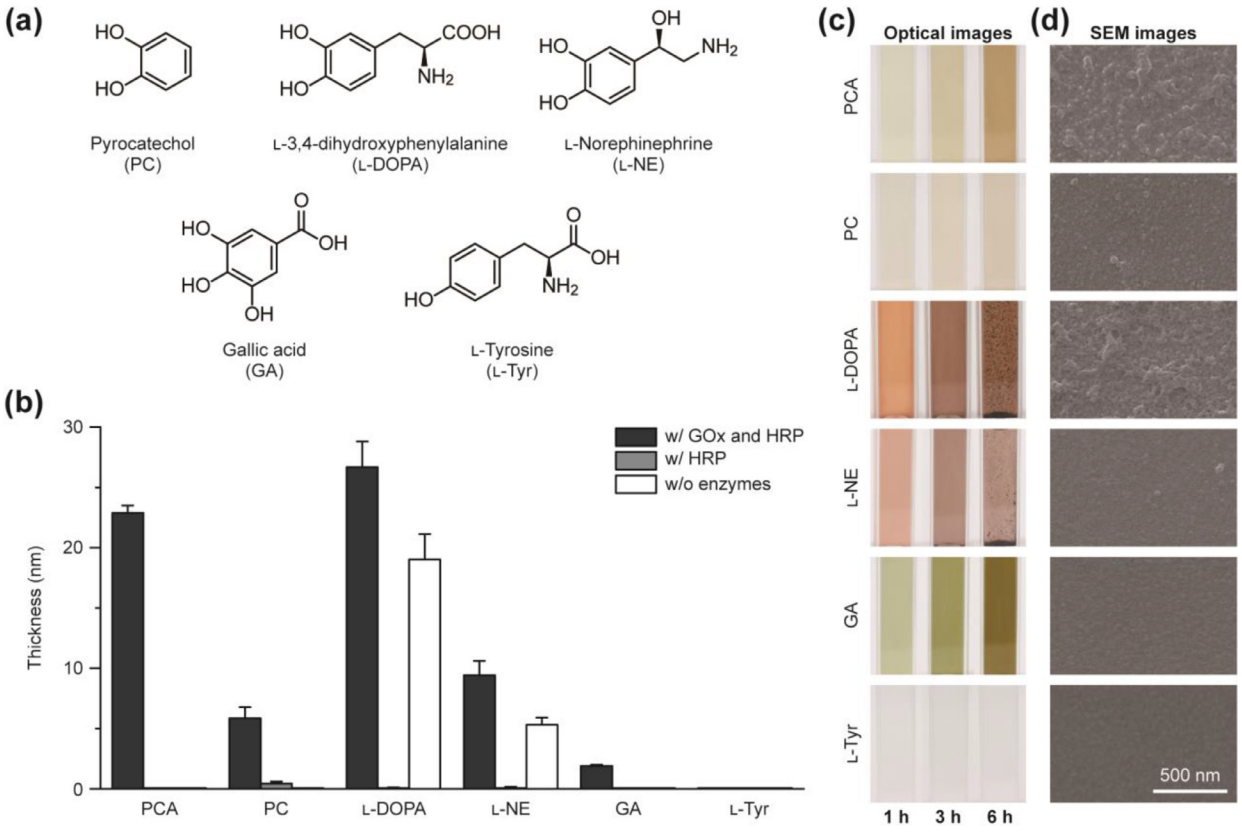

Fig. 4. (a) Molecular structures of PC, L-DOPA, L-NE, GA, and L-Tyr. (b) Film thickness graph for $MLS_{[PCA]}$, $MLS_{[PC]}$, $MLS_{[L\text{-}DOPA]}$, $MLS_{[L\text{-}NE]}$, $MLS_{[GA]}$, and $MLS_{[L\text{-}Tyr]}$. The film formation was performed (black) with GOx/HRP/Glu, (gray) with HRP/H_2O_2, and (white) without enzymes (pH 7.4). (c) Optical images of the reaction solutions after 1, 3, and 6 h of incubation. (d) SEM micrographs of Au substrates after 6 h of reaction.

of 283.6 (C–C and C–H), 284.9 (C–O), and 287.1 eV (C=O), indicative of the $MLS_{[PCA]}$ film formation (Fig. 3e).

In contrast, no $MLS_{[PCA]}$ films were formed in the absence of the enzymes, confirmed by the ellipsometric, PIERS, and XPS analyses (Fig. S2). For example, no thickness increase was observed even after 6 h of reaction (triangles on Fig. 3a). We also found that neither HRP and H_2O_2 nor GOx and Glu formed films. These results arguably confirmed that the combination of GOx and HRP, developed herein, was critically required for $MLS_{[PCA]}$ film formation.

On the other hand, the $MLS_{[L\text{-}DOPA]}$ film grew continuously in a linear fashion (Fig. S3). The film thickness was 1.96 nm after 1 h of reaction and increased to 26.7 nm at 6 h. The PIERS spectrum, showing the peaks at 1326 for amine groups (C–N), 1623 for carbonyl ones (C=O), and 3270 cm^{-1} for hydroxyl (O–H) ones, confirmed the $MLS_{[L\text{-}DOPA]}$ film formation. The deconvoluted C 1s XPS peaks at 283.7 (C–C and C–H), 285.0 (C–O and C–N), and 287.3 eV (C=O and C=N) further confirmed the film formation. Taken all together, our enzymatic cascade reaction system facilitated the formation of MLS films, from *o*-diphenols with or without amine groups, and widened the substrate scope for melanogenesis-mimetic film formation.

3.3. Substrate scope for MLS film formation

The current enzyme system was designed to be capable of catalyzing the MLS formation from various *o*-diphenols. As aforementioned, tyrosinase converts monophenols to diphenols (via one-electron oxidation) and oxidizes catecholamines to their quinones (via two-electron oxidation) in biological melanogenesis, but its in-vitro generation of MLS is limited to phenolic amines as a substrate [22].

To further investigate the substrate scope, we first employed pyrocatechol (benzene-1,2-diol, PC), which is the simplest *o*-diphenol (Fig. 4a). We also tested phenolic amines as a reaction precursor in order to study the similarities and differences among reaction precursors in the enzyme-mediated MLS film formation. Specifically, we chose L-Tyr, L-DOPA, and L-norepinephrine (L-NE), which were reported to form the MLS films by the action of tyrosinase [22]. We additionally added gallic acid (3,4,5-trihydroxybenzoic acid, GA) to the test set.

The ellipsometric analysis showed that our enzymatic system formed thin films from PC, L-DOPA, L-NE, and GA, but not from L-Tyr. After 6 h of reaction, the film thickness was measured to be 5.8 nm for $MLS_{[PC]}$, 26.8 nm for $MLS_{[L\text{-}DOPA]}$, 9.4 nm for $MLS_{[L\text{-}NE]}$, and 1.9 nm for $MLS_{[GA]}$, respectively (Fig. 4b). It has been reported that HRP could catalyze the polymerization of 4-hydroxyphenylacetic acid (HPA) in the presence of H_2O_2 and construct nanometer-thick poly(HPA) films and capsules [34]. No films were formed with L-Tyr in our system, presumably because the first step in melanogenesis—hydroxylation of L-Tyr to L-DOPA—was not achievable in the system of GOx and HRP.

We performed control experiments to investigate the reaction characteristics in detail. In the PBS solution (pH 7.4) without GOx and HRP, L-DOPA and L-NE formed thinner films than the ones in the GOx/HRP system: for example, 26.8 nm vs. 19.0 nm for L-DOPA and 9.4 nm vs. 5.3 nm for L-NE after 6 h of reaction. In contrast, no films were formed from PC and GA in the PBS solution, showing that the enzymes were required for film formation in this case. In the case of L-DOPA and L-NE, it could undergo self-oxidation in the presence of molecular oxygen, followed by intramolecular cyclization, leading to the production of MLS [16]. We also used HRP and H_2O_2 for film formation, and found that none of the four compounds (PC, L-DOPA, L-NE, and GA) formed films. We thought that rapid oxidation of the compounds by HRP led to uncontrollable production of MLS and undesired precipitation. As expected, the use of GOx and Glu did not form the films. The control experiments clearly confirmed that the combination of GOx and HRP was required for the MLS film formation in a controlled fashion.

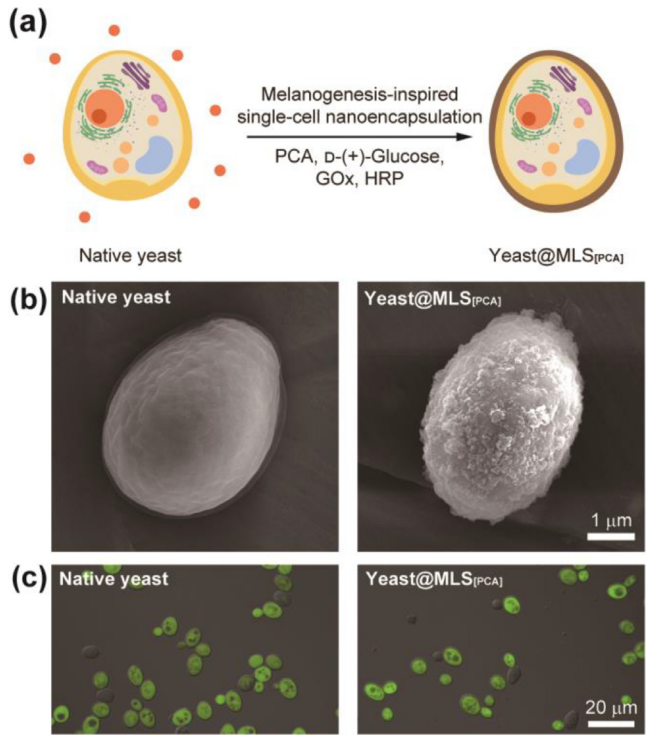

Fig. 5. (a) Schematic for $MLS_{[PCA]}$ shell formation in SCNE. (b) SEM and (c) CLSM images of native yeast and yeast@$MLS_{[PCA]}$.

It is known that the structural differences of melanin in nature lead to their diversified color ranges and surface morphologies [25], which was also observed in our system (Fig. 4c,d). The color of matured MLS solutions was significantly different from each other depending on the precursors used. For example, the color of the $MLS_{[PCA]}$ solution was much darker than that of the $MLS_{[PC]}$ solution. We thought that this color difference might result from the aldehyde group in PCA, which could allow for additional cross-linking reactions, such as benzoin condensation, while polymerization of PC is limited on the formation of C–C and C–O–C bonds between aromatic rings [35–37]. These results indicated that the MLS films and shells with varied physicochemical properties could be formed by the expanded substrate scope [38], which would be beneficial in the nanoarchitectonic creation of cell-in-shell structures in SCNE.

3.4. *Single-cell nanoencapsulation (SCNE) of* S. cerevisiae

We applied the reaction protocol of $MLS_{[PCA]}$ production to SCNE of *S. cerevisiae* as a proof-of-demonstration (Fig. 5a). In this experimentation, we particularly intended to mimic the stimuli-responsive, autonomous formation of MLS coats found in certain yeast, such as *Cryptococcus neoformans*, for the enhanced resistance against external stressors [10]. Briefly, a pellet of *S. cerevisiae* was mixed with the enzyme-mediated reaction solution (0.4 mg mL^{-1} of PCA; [Glu] = 10 mM; 0.5 U mL^{-1} of GOx; 0.1 U mL^{-1} of HRP), the mixture was incubated at 33 °C for 6 h, and resulting yeast@$MLS_{[PCA]}$ were collected for characterizations. The SEM image after SCNE indicated that the $MLS_{[PCA]}$ shells were successfully formed on individual *S. cerevisiae* (Fig. 5b). Mechanisms on the $MLS_{[PCA]}$ shell formation on individual *S. cerevisiae* would involve the substrate-independent adhesiveness of catechol-based MLS and the cross-linking reactions of intermediates, *o*-quinones, with amines and thiols on the cell surface via Michael-type addition and Schiff base reactions [4,39]. The shell formation was stimuli-responsive: no shells were formed without the Glu supply to the system.

The thickness and permeability of the $MLS_{[PCA]}$ shells were further investigated. We constructed the $MLS_{[PCA]}$ shells on polystyrene (PS) beads (diameter: 3.97 μm) and dissolved the sacrificial PS templates with THF to produce the hollow $MLS_{[PCA]}$ capsules. The shell thickness was measured to be 10.1 nm on average by AFM (Fig. S4). The permeability of $MLS_{[PCA]}$ capsules was investigated with FITC-conjugated dextrans with various molecular weights (MWs), in which the capsules allowed the penetration of low-MW (4 and 20 kDa) dextrans, but not for high-MW (250 kDa) one (Fig. S5). This permselective characteristic of nanometric $MLS_{[PCA]}$ shells might enable the selective transfer of oxygen, nutrients, and cell metabolites, while the shells shun large molecules, such as lytic enzymes, and antibodies.

It is a pre-requisite for SCNE to ensure that the materials and processes do not harm to living cells. In this regard, the cell viability after SCNE with $MLS_{[PCA]}$ was studied by the fluorescein diacetate (FDA) assay, in which FDA was converted to green-fluorescent fluorescein by intracellular esterases in viable cells (Fig. 5c). The viability was calculated to be 73.5% (viability of native yeast: 99.2%), confirming the cytocompatibility of our enzymatic system (Fig. 5c). As a comparison, the air-oxidative polydopamine shell formation for *S. cerevisiae* was reported to be ~54% [13]. Based on the results, it could be concluded that the enzyme combination of GOx and HRP expanded the chemical tools for manipulating living cells at the single-cell level.

4. Conclusions

In summary, we developed an enzymatic cascade system for forming melanin-like films and shells from various *ortho*-diphenols. Especially, our system of glucose oxidase (GOx) and horseradish peroxidase (HRP) was found to be capable of polymerizing amine-absent *ortho*-diphenols, such as protocatechuic aldehyde and pyrocatechol.

The system developed herein has advantages and disadvantages. It expands the substrate scope for melanin-mimetic film formation, which would lead to varied physicochemical properties of the films and shells. The physicochemical properties would be further diversified by the incorporation of other compounds to the melanin structure, as noticed in the pheomelanin formation [40–42]. The system is stimuli-responsive. The shell formation is glucose-dependent. It is anticipated that yeast cells would autonomously arm themselves with melanin-based shells during their division in the presence of the nutrient, glucose. Enzymatic systems could be further designed to be stimuli-responsive and autonomous for other cell types including mammalian cells in the shell formation. On the other hand, the GOx/HRP system is observed to be toxic to the cells to some extent, although the viability after SCNE of *S. cerevisiae* is legitimately high. The reaction optimization, along with the use of other *ortho*-diphenols than protocatechuic aldehyde, would be required for fully cytocompatible SCNE, which is our next research thrust.

Compared with the layer-by-layer (LbL) approach that has intensively been used for SCNE, [43–45] the approach developed herein is simple and fast, not requiring the repeated deposition steps, as well as potentially providing advantageous properties in SCNE, such as neutralization of reactive oxygen species and other radicals, shielding of UV radiation, and inactivation of microbicidal activities. Considering the potential utility of melanin-inspired materials, our strategy would provide an advanced tool for diversifying melanin-like materials in the biomedical sector. We also believe that this work promises advances in the nanoarchitectonic SCNE that integrates innate enzymatic reactions in cells with chemically provided enzymatic reactions in shells and/or outside for reprogrammed metabolic activities and rewired reaction pathways [46–48].

Declaration of Competing Interest

The authors declare that they have no known competing financial interests or personal relationships that could have appeared to influence the work reported in this paper.

Acknowledgments

This work was supported by Hansol Poultry, Inc. and the 2020 Research Fund of University of Ulsan.

Supplementary materials

Supplementary material associated with this article can be found, in the online version, at doi:10.1016/j.apsadv.2021.100098.

References

[1] R.R. Naik, S. Singamaneni, Introduction: bioinspired and biomimetic materials, Chem. Rev. 117 (2017) 12581–12583, doi:10.1021/acs.chemrev.7b00552.
[2] C. Zhang, D.A. Mcadams II, J.C. Grunlan, Nano/micro-manufacturing of bioinspired materials: a review of methods to mimic natural structures, Adv. Mater. 28 (2016) 6292–6321, doi:10.1002/adma.201505555.
[3] U.G.K. Wegst, H. Bai, E. Saiz, A.P. Tomsia, R.O. Ritchie, Bioinspired structural materials, Nat. Mater. 14 (2015) 23–36, doi:10.1038/nmat4089.
[4] H. Lee, S.M. Dellatore, W.M. Miller, P.B. Messersmith, Mussel-inspired surface chemistry for multifunctional coatings, Science 318 (2007) 426–430, doi:10.1126/science.1147241.
[5] B.J. Kim, H. Cho, J.H. Park, J.F. Mano, I.S. Choi, Strategic advances in formation of cell-in-shell structures: from syntheses to applications, Adv. Mater. 30 (2018) 1706063, doi:10.1002/adma.201706063.
[6] J.H. Park, D. Hong, J. Lee, I.S. Choi, Cell-in-shell hybrids: chemical nanoencapsulation of individual cells, Acc. Chem. Res. 49 (2016) 792–800, doi:10.1021/acs.accounts.6b00087.
[7] R.F. Fakhrullin, Y.M. Lvov, "Face-lifting" and "make-up" for microorganisms: layer-by-layer polyelectrolyte nanocoating, ACS Nano 6 (2012) 4557–4564, doi:10.1021/nn301776y.
[8] H. Tang, Regulation and function of the melanization reaction in drosophila, Fly 3 (2009) 105–111, doi:10.4161/fly.3.1.7747.
[9] J. Nakhleh, L.E. Moussawi, M. A. Osta, Chapter three - the melanization response in insect immunity, Adv. Insect Physiol. 52 (2017) 83–109, doi:10.1016/bs.aiip.2016.11.002.
[10] D. Lee, E.-H. Jang, M. Lee, S.-W. Kim, Y. Lee, K.-T. Lee, Y.-S. Bahn, Unraveling melanin biosynthesis and signaling networks in *Cryptococcus neoformans*, mBio 10 (2019) e02267–19, doi:10.1128/mBio.02267-19.
[11] R.J.B. Cordero, E. Camacho, A. Casadevall, Melanization in *Cryptococcus neoformans* requires complex regulation, mBio 11 (2020) e03313–19, doi:10.1128/mBio.03313-19.
[12] M. Brenner, V.J. Hearing, The protective role of melanin against UV damage in human skin, Photochem. Photobiol. 84 (2008) 539–549, doi:10.1111/j.1751-1097.2007.00226.x.
[13] S.H. Yang, S.M. Kang, K.-B. Lee, T.D. Chung, H. Lee, I.S. Choi, Mussel-inspired encapsulation and functionalization of individual yeast cells, J. Am. Chem. Soc. 133 (2011) 2795–2797, doi:10.1021/ja1100189.
[14] P. Meredith, T. Sarna, The physical and chemical properties of eumelanin, Pigment Cell Res. 19 (2006) 572–594, doi:10.1111/j.1600-0749.2006.00345.x.
[15] S. Ito, K. Wakamatsu, Chemistry of mixed melanogenesis—pivotal roles of dopaquinone, Photochem. Photobiol. 84 (2008) 582–592, doi:10.1111/j.1751-1097.2007.00238.x.
[16] C.J. Vavricka, B.M. Christensen, J. Li, Melanization in living organisms: a perspective of species evolution, Protein Cell 1 (2010) 830–841, doi:10.1007/s13238-010-0109-8.
[17] N. Wang, D.N. Hebert, Tyrosinase maturation through the mammalian secretory pathway: bringing color to life, Pigment Cell Res. 19 (2006) 3–18, doi:10.1111/j.1600-0749.2005.00288.x.
[18] V.J. Hearing, M. Jiménez, Mammalian tyrosinase—the critical regulatory control point in melanocyte pigmentation, Int. J. Biochem. 19 (1987) 1141–1147, doi:10.1016/0020-711X(87)90095-4.
[19] C. Olivares, C. Jiménez-Cervantes, J.A. Lozano, F. Solano, J.C. García-Borrón, The 5, 6-dihydroxyindole-2-carboxylic acid (DHICA) oxidase activity of human tyrosinase, Biochem. J. 354 (2001) 131–139, doi:10.1042/bj3540131.
[20] Y. Matoba, T. Kumagai, A. Yamamoto, H. Yoshitsu, M. Sugiyama, Crystallographic evidence that the dinuclear copper center of tyrosinase is flexible during catalysis, J. Biol. Chem. 281 (2006) 8981–8990, doi:10.1074/jbc.M509785200.
[21] M. D'Ischia, Melanin-based functional materials, Int. J. Mol. Sci. 19 (2018) 228–231, doi:10.3390/ijms19010228.
[22] J.Y. Kim, W.I. Kim, W. Youn, J. Seo, B.J. Kim, J.K. Lee, I.S. Choi, Enzymatic film formation of nature-derived phenolic amines, Nanoscale 10 (2018) 13351–13355, doi:10.1039/C8NR04312D.
[23] T. Liu, Y. Wang, W. Zhong, B. Li, K. Mequanint, G. Luo, M. Xing, Biomedical applications of layer-by-layer self-assembly for cell encapsulation: current status and future perspectives, Adv. Healthc. Mater. 8 (2019) 1800939, doi:10.1002/adhm.201800939.
[24] M.B. Oliveria, J. Hatami, J.F. Mano, Coating strategies using layer-by-layer deposition for cell encapsulation, Chem. Asian J. 11 (2016) 1753–1764, doi:10.1002/asia.201600145.
[25] J.D. Simon, D.N. Peles, The red and the black, Acc. Chem. Res. 43 (2010) 1452–1460, doi:10.1021/ar100079y.
[26] J.D. Nosanchuk, A.L. Rosas, S.C. Lee, A. Casadevall, Melanisation of *Cryptococcus neoformans* in human brain tissue, Lancet 355 (2000) 2049–2050, doi:10.1016/S0140-6736(00)02356-4.
[27] U. Perez-Cuesta, L. Aparicio-Fernandez, X. Guruceaga, L. Martin-Souto, A. Abad-Diaz-De-Cerio, A. Antoran, I. Buldain, F.L. Hernando, A. Ramirez-Garcia, A. Rementeria, Melanin and pyomelanin in *Aspergillus fumigatus*: from its genetics to host interaction, Int. Microbiol. 23 (2020) 55–63, doi:10.1007/s10123-019-00078-0.
[28] M.E. Pavan, N.I. López, M.J. Pettinari, Melanin biosynthesis in bacteria, regulation and production perspectives, Appl. Microbiol. Biotechnol. 104 (2020) 1357–1370, doi:10.1007/s00253-019-10245-y.
[29] S.O. Andersen, Insect cuticular sclerotization: a review, Insect Biochem. Mol. Biol. 40 (2010) 166–178, doi:10.1016/j.ibmb.2009.10.007.
[30] F. Solano, Melanins: skin pigments and much more—types, structural models, biological functions, and formation routes, New J. Sci. 2014 (2014) 1–28, doi:10.1155/2014/498276.
[31] J. Li, M.A. Barid, M.A. Davis, W. Tai, L.S. Zweifel, K.M. Adams, A. Waldorf, M. Gale Jr, L. Rajagopal, R.H. Pierce, X. Gao, Dramatic enhancement of the detection limits of bioassays via ultrafast deposition of polydopamine, Nat. Biomed. Eng. 1 (2017) 0082, doi:10.1038/s41551-017-0082.
[32] M. Sugumaran, V. Semensi, H. Dali, K. Nellaiappan, Oxidation of 3,4-dihydroxybenzyl alcohol: a sclerotizing precursor for cockroach ootheca, Arch. Insect Biochem. Physiol. 16 (1991) 31–44, doi:10.1002/arch.940160105.
[33] U.V. Mahilny, A.V. Trofimova, A new mechanism of stable optical birefringence recording under polarized UV radiation in photocrosslinking polymeric materials, J. Opt. 13 (2011) 105601, doi:10.1088/2040-8978/13/10/105601.
[34] T. Shutava, Z. Zheng, V. John, Y. Lvov, Microcapsule modification with peroxidase-catalyzed phenol polymerization, Biomarcomolecules 5 (2004) 914–921, doi:10.1021/bm034476x.
[35] Y. Liu, S. Sakai, S. Kawa, M. Taya, Identification of hydrogen peroxide-secreting cells by cytocompatible coating with a hydrogel membrane, Anal. Chem. 86 (2014) 11592–11598, doi:10.1021/ac503342k.
[36] Y. Zhao, M. Fan, Y. Chen, Z. Liu, C. Shao, B. Jin, X. Wang, L. Hui, S. Wang, Z. Liao, D. Ling, R. Tang, B. Wang, Surface-anchored framework for generating RhD-epitope stealth red blood cells, Sci. Adv. 6 (2020) eaaw9679, doi:10.1126/sciadv.aaw9679.
[37] H.S. Mason, The chemistry of melanin; mechanism of the oxidation of dihydroxyphenylalanine by tyrosinase, J. Biol. Chem. 172 (1948) 83–99, doi:10.1016/S0021-9258(18)35614-X.
[38] J. Hong, S. Choi, D.G. Jwa, M. Kim, S.M. Kang, Mussel-inspired, one-step thiol functionalization of solid surfaces, Langmuir 36 (2020) 1608–1614, doi:10.1021/acs.langmuir.9b03646.
[39] S.-H. Kim, S.-H. Lee, J.-E. Lee, S.J. Park, K. Kim, I.S. Kim, Y.-S. Lee, N.S. Hwang, B.-G. Kim, Tissue adhesive, rapid forming, and sprayable ECM hydrogel via recombinant tyrosinase crosslinking, Biomaterials 178 (2018) 401–412, doi:10.1016/j.biomaterials.2018.04.057.
[40] W. Jeong, E. Kim, J. Jeong, H. Bisht, H. Kang, D. Hong, Development of stimulus-responsive degradable film via codeposition of dopamine and cystamine, Chem. Asian J. 15 (2020) 2622–2626, doi:10.1002/asia.202000216.
[41] T. Schneider, V. Kubyshkin, N. Budisa, Synthesis of a photo-caged DOPA derivative by selective alkylation of 3,4-dihydroxybenzaldehyde, Eur. J. Org. Chem. 2018 (2018) 2053–2063, doi:10.1002/ejoc.201701749.
[42] S.M. Kang, N.S. Hwang, J. Yeom, S.Y. Park, P.B. Messersmith, I.S. Choi, R. Langer, D.G. Anderson, H. Lee, One-step multipurpose surface functionalization by adhesive catecholamine, Adv. Funct. Mater. 22 (2012) 2949–2955, doi:10.1002/adfm.201200177.
[43] B. Franz, S.S. Balkundi, C. Dahl, Y.M. Lvov, A. Prange, Layer-by-layer nanoencapsulation of microbes: controlled cell surface modification and investigation of substrate uptake in bacteria, Macromol. Biosci. 10 (2010) 164–172, doi:10.1002/mabi.200900142.
[44] S.A. Konnova, Y.M. Lvov, R.F. Fakhrullin, Nanoshell assembly for magnet-responsive oil-degrading bacteria, Langmuir 32 (2016) 12552–12558, doi:10.1021/acs.langmuir.6b01743.
[45] S.A. Konnova, A.A. Danilushkina, G.I. Fakhrullina, F.S. Akhatova, A.R. Badrutdinov, R.F. Fakhrullin, Silver nanoparticle-coated "cyborg" microorganisms: rapid assembly of polymer-stabilised nanoparticles on microbial cells, RSC Adv. 5 (2015) 13530–13537, doi:10.1039/C4RA15857A.
[46] W. Youn, J.Y. Kim, J. Park, N. Kim, H. Choi, H. Cho, I.S. Choi, Single-cell nanoencapsulation: from passive to active shells, Adv. Mater. 32 (2020) 1907001, doi:10.1002/adma.201907001.
[47] K. Liang, J.J. Richardson, C.J. Doonan, X. Mulet, Y. Ju, J. Cui, F. Caruso, P. Falcaro, An enzyme-coated metal–organic framework shell for synthetically adaptive cell survival, Angew. Chem. Int. Ed. 56 (2017) 8510–8515, doi:10.1002/anie.201704120.
[48] D. Su, J. Qi, X. Liu, L. Wang, H. Zhang, H. Xie, X. Huang, Enzyme-modulated anaerobic encapsulation of chlorella cells allows switching from O_2 to H_2 production, Angew. Chem. Int. Ed. 131 (2019) 4032–4035, doi:10.1002/ange.201900255.